AGU ADVANCING EARTH AND SPACE SCIENCE

Geophysical Research Letters®

RESEARCH LETTER
10.1029/2021GL093979

Key Points:

- We document a complex 3D source migration process with delayed mainshock triggering that is controlled by a local hydrogeological setting
- Poroelastic effects contribute to induced events but are probably insufficient to activate a large fault segment not critically stressed
- Rapid pore-pressure build-up can be very localized and lead to large earthquakes if adequate hydrological paths exist

Supporting Information:

Supporting Information may be found in the online version of this article.

Correspondence to:

H. Kao,
honn.kao@canada.ca

Citation:

Gao, D., Kao, H., Wang, B., Visser, R., Schultz, R., & Harrington, R. M. (2022). Complex 3D migration and delayed triggering of hydraulic fracturing-induced seismicity: A case study near Fox Creek, Alberta. *Geophysical Research Letters*, *49*, e2021GL093979. https://doi.org/10.1029/2021GL093979

Received 20 APR 2021
Accepted 10 DEC 2021

Complex 3D Migration and Delayed Triggering of Hydraulic Fracturing-Induced Seismicity: A Case Study Near Fox Creek, Alberta

Dawei Gao[1,2], Honn Kao[1,2], Bei Wang[1,2], Ryan Visser[2], Ryan Schultz[3], and Rebecca M. Harrington[4]

[1]School of Earth and Ocean Sciences, University of Victoria, Victoria, BC, Canada, [2]Pacific Geoscience Centre, Geological Survey of Canada, Sidney, BC, Canada, [3]Department of Geophysics, Stanford University, Stanford, CA, USA, [4]Ruhr University Bochum, Institute of Geology, Mineralogy, and Geophysics, Bochum, Germany

Abstract Earthquakes resulting from hydraulic fracturing (HF) can have delayed triggering relative to injection commencement over a varied range of time scales, with the majority of $M \geq 4$ mainshocks occurring near/after well completion. This poses serious challenges for risk mitigation and hazard assessment. Here, we document a high-resolution, three-dimensional source migration process with delayed mainshock triggering that is controlled by local hydrogeological conditions near Fox Creek, Alberta, Canada. Our results reveal that poroelastic effects might contribute to induced seismicity, but are probably insufficient to activate a large fault segment not critically stressed. The rapid pore-pressure build-up from HF can be very localized and capable of producing large, felt earthquakes if adequate hydrological paths exist. We interpret the delayed triggering as a manifestation of pore-pressure build-up along pre-existing faults needed to facilitate seismic failure. Our findings can explain why so few injection operations are seismogenic.

Plain Language Summary Fluid injection-induced earthquakes (IIE), especially those $M \geq 4$ mainshocks, are often observed to occur near or after well completion. Such delayed triggering relative to injection commencement poses serious challenges for both regulators and the energy industry to establish an effective mitigation strategy for the potential seismic risk. In this study, we reveal a high-resolution, complex three-dimensional pattern of IIE migration near Fox Creek, Alberta, Canada. The observed first-outward-then-inward IIE sequence highlights the significance of hydrogeological networks in facilitating fluid pressure migration and the associated seismic failure. The detailed spatiotemporal distribution of IIE suggests that the effect of pore-pressure build-up from hydraulic fracturing (HF) can be very localized. The delayed triggering is a combined result of the fluid pressure migration and the current stress state of the hosting fault system away from the HF wells. The findings from this study also provide plausible explanations on why only a very limited number of fluid injections are seismogenic.

1. Introduction

Fluid injection-induced earthquakes (IIE), especially relatively large ones, are often observed to have delayed triggering relative to injection commencement. For long-term wastewater disposal (WD), the delay time (i.e., time lag between the initiation of injection and the onset of induced seismicity) can be as long as decades (Keranen et al., 2013). For relatively short-term hydraulic fracturing (HF) operations, the delay time varies from hours to weeks (e.g., Bao & Eaton, 2016; Fasola et al., 2019). In many cases, the largest events, generally with $M \geq 4$, occur near or after well completion (e.g., Lei et al., 2017; Peña Castro et al., 2020; Schultz et al., 2020, 2017; Schultz & Wang, 2020; Wang et al., 2017) which severely challenges the designing of an effective risk mitigation strategy. Understanding the controlling factor(s) of the delayed triggering of significant IIE is of paramount importance. However, the underlying physics is surprisingly far from clear due to limited observations and/or incomplete injection databases.

The 2015 Mw 3.9 earthquake sequence near Fox Creek, Alberta, Canada is the first well-known delayed HF-induced case with a ~2-week gap between the stimulation completion and the mainshock. The local seismograph array data contributed by the industry enables precise determination of earthquake hypocenters in comparison to other induced seismicity studies which often rely on regional stations (Bao & Eaton, 2016). During the post-stimulation process, only ~7% of the injected fluids, in contrast to a typical value of ~50% in western Canada, were

recovered, unambiguously indicating that a tremendous amount of fluid has leaked off into nearby fault zones (Bao & Eaton, 2016). Given the robust earthquake locations, comprehensive stimulation database, and large volume of fluid loss, the 2015 Fox Creek sequence provides a unique opportunity to infer the corresponding three-dimensional (3D) fluid migration process and the spatiotemporal interactions between the hosting structures and injected fluid at an unpreceded resolution.

According to Bao and Eaton (2016), the Coulomb stress change (ΔCFS) due to fracture opening and pore-pressure diffusion is responsible for the earlier events that occurred during the HF stimulation (referred to as the east sequence) and the delayed post-stimulation events (west sequence, including the Mw 3.9 strike-slip mainshock), respectively (Figure 1a). However, this model has at least two serious issues. First, it is inconsistent with the observed chronological sequence of stimulation and seismicity. There are two periods of stage stimulation from north to south with a ~1-week gap (Figure 1). The earliest event (i.e., the east sequence) actually occurred about 2 days after the last stage of the first stimulation period (P1 in Figure 1b). This is contradictory to their assumed elastic stress triggering mechanism, which should be instantaneous. Instead, the 2-day delay suggests that pressure migration might have begun during or shortly after P1. Moreover, the west sequence seems to initiate at a greater depth relative to the injection well with a clear upward trend of propagation (Bao & Eaton, 2016). Hence it is very unlikely that the west sequence was caused by downward pressure migration along a near-vertical permeable fault with fluids originating from the wellbore directly above (Figure 1a).

Second, the initial model results in an overestimation of static ΔCFS in triggering the earlier events (east sequence). The sudden increase of seismicity of the east sequence (including an Mw 3.2 earthquake) happened halfway through the second stimulation period (P2 in Figure 1b) when the treatment approached the vertical fault hosting the seismicity sequence (stages 14 and 15 of well 2 in Figure 1a). Thus, the actual ΔCFS in triggering these events is significantly overestimated by simply summing the effects of all HF stages. Furthermore, the extremely large injected volume (~50% more) and long duration (~5.75 times longer) of stage 14 compared with other stages suggest the likely start time of serious fluid leakage (Figure 1b) (Peña Castro et al., 2020). Consequently, it is inappropriate to calculate the net ΔCFS by ignoring the effect of pore-pressure diffusion with the assumption that the total fracture (opening) volume equals the total volume of injected fluid (Bao & Eaton, 2016).

Here we revisit the 2015 Fox Creek sequence with tight constraints from local geological structures and injection parameters. We first employ waveform cross-correlation and hierarchical clustering analysis to identify near-identical events with highly similar waveforms that are presumably associated with the same seismogenic structures. Events with low values of cross-correlation coefficient (CC) with respect to major event clusters might be related to nearby fractures or subsidiary faults with different orientations and/or focal mechanisms, and therefore are excluded from our interpretation. We then analyze the spatiotemporal evolution of those on-fault events. By taking advantage of the complete HF stimulation database, we further conduct poroelastic modeling to investigate the delayed triggering process. Our results reveal a high-resolution, complex 3D pattern of IIE migration that is probably controlled by local fault architecture and its hydrogeological properties. Finally, we discuss the broad implications of this study.

2. Methods

2.1. Waveform Cross-Correlation and Hierarchical Clustering Analysis

Near-identical waveforms between events are commonly interpreted as an indication of a similar source location and focal mechanism (Schultz et al., 2014). In this study, we begin by adopting the relocated earthquake catalog (69 events in total) from Bao and Eaton (2016) (see details in Text S1; Figures S1 and S2). The overall pattern of relative location among hypocenters of these events is deemed robust with relative location uncertainty generally less than 10 and 30 m in the horizontal and vertical directions, respectively (Figure S2). We note that the overall seismic pattern remains essentially the same even if the relative location uncertainty is assumed to be underestimated by a factor of 5 (Figure 2). Next, we perform pair-wise waveform cross-correlation and clustering analysis (Hayward & Bostock, 2017; Schultz et al., 2014, 2015, 2017) to identify events with highly similar waveforms that presumably occurred on the same fault segments.

The waveform similarity can be quantitatively characterized by CC values. Since data availability of the private seismograph array used by prior work (Bao & Eaton, 2016) is restricted, we choose to calculate the CC values between event pairs with seismograms from the station BRLDA (Figure 1a) that have a generally high

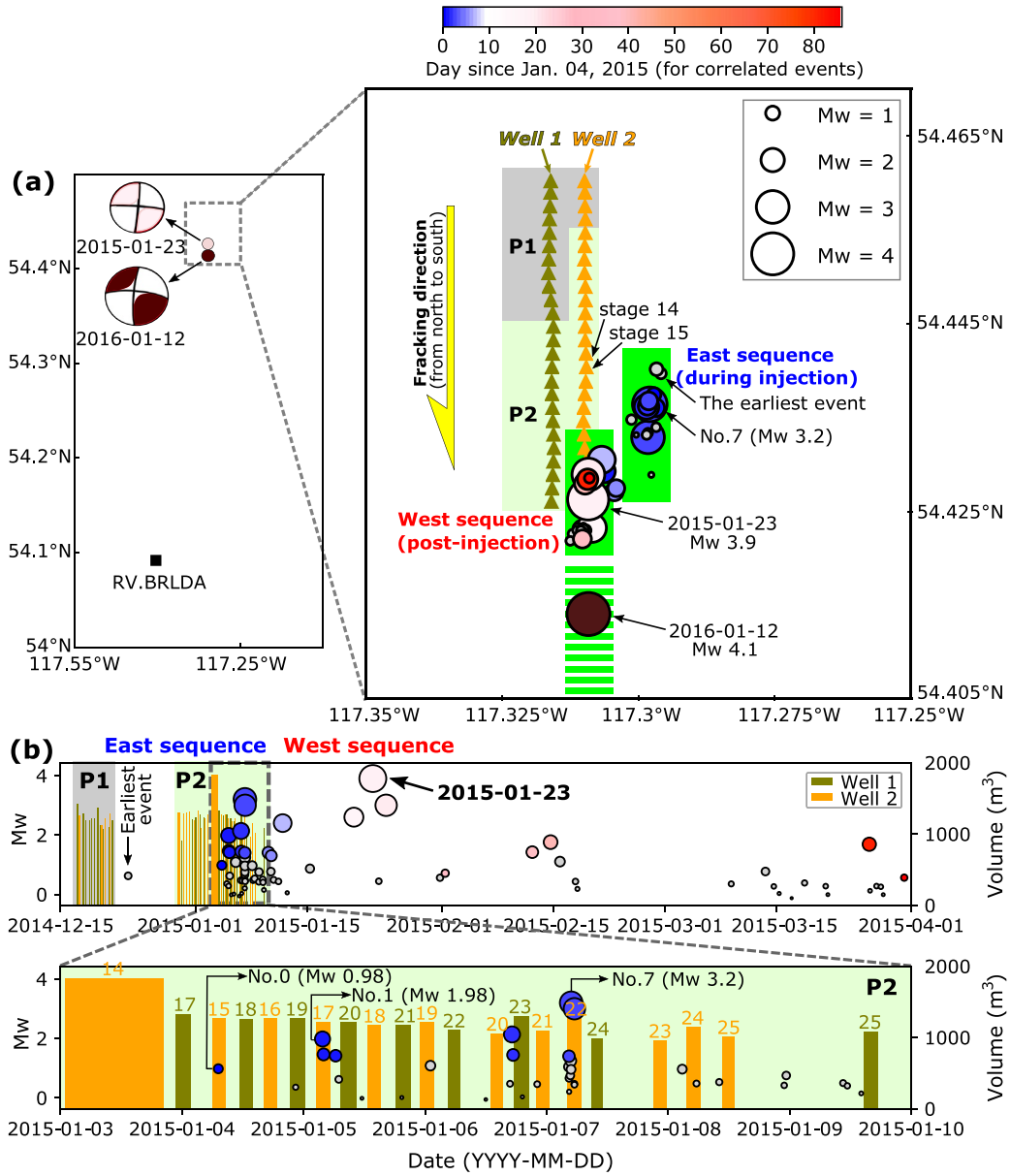

Figure 1. Injection-induced earthquakes in the Fox Creek area, Alberta, Canada. (a) Map showing the geographic location of the 2015 Mw 3.9 and 2016 Mw 4.1 earthquake sequences. Beach balls of the two mainshocks are taken from prior work (Schultz et al., 2017). The black square in the left panel shows the seismic station used in this study. In the right panel, solid lime bars denote the two fault strands of the 2015 sequence; dashed lime bar marks the hosted fault of the 2016 Mw 4.1 event; triangles represent hydraulic fracturing stages. (b) Injection history is associated with the occurrence of induced earthquakes. The height of each colored bar represents the total volume of fluid injected at each stage while the width depicts the stage duration. In the bottom panel, the stage ID is labeled above each treatment. In both (a) and (b), correlated (near-identical) events are plotted chronologically from blue to red, whereas gray circles represent uncorrelated small events. Gray and pale-green shaded areas correspond to P1 and P2 injection periods, respectively.

signal-to-noise ratio (Schultz et al., 2017) and are publicly accessible from Incorporated Research Institutions for Seismology (http://ds.iris.edu/ds/nodes/dmc/forms/breqfast-request/, last accessed July 2020). The technical details of the CC calculation are presented in Text S2.

The aforementioned pair-wise cross-correlation yields a $[69 \times 69]$ similarity matrix. We obtain the near-identical events by implementing a hierarchical clustering algorithm based on the unweighted pair group method using the average approach (UPGMA), available as a SciPy package (Jones et al., 2001; https://docs.scipy.org). Compared

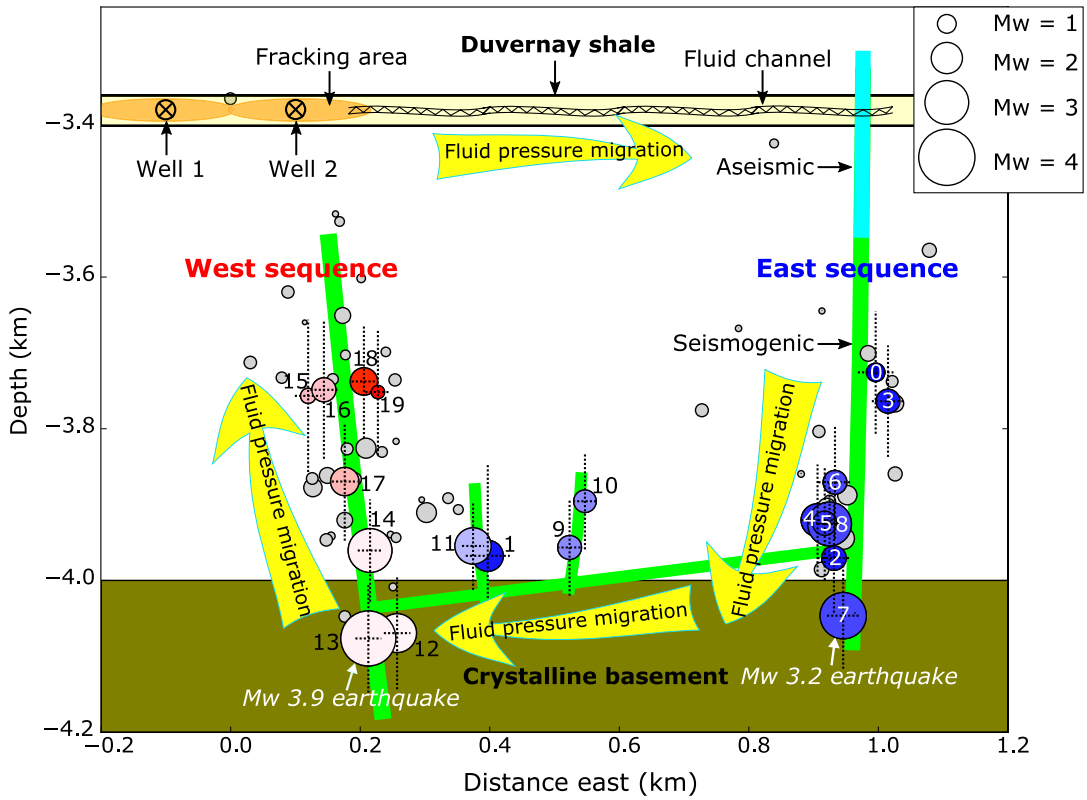

Figure 2. East-west cross section of the 2015 Mw 3.9 earthquake sequence. Twenty correlated events are marked by numbered and color-coded circles, with the smaller numbers and cooler colors corresponding to earlier events. Color scheme for the event symbol is the same as that of Figure 1. Dotted lines denote the reported location uncertainties exaggerated by a factor of 5. Gray circles represent the 49 poorly correlated events. Circle sizes are scaled according to earthquake magnitudes. Crossed circles mark two hydraulic fracturing horizontal wells.

with the "chain-like" methods (e.g., Igarashi et al., 2003), the UPGMA method yields more robust results in grouping earthquakes (Hayward & Bostock, 2017). Here we define a cluster as a group of events in which the CC of all pairs are higher than 0.75 (Figure S3a). Such a CC threshold, the same as the value used in other IIE related clustering studies (Cauchie et al., 2020; Schultz et al., 2014), is determined by visually inspecting the waveforms in the corresponding cluster. Eventually, we obtain 1 cluster with 20 near-identical events. The high waveform similarity among these events, including the coda train (Figure S3b), justifies our choice of the threshold value.

2.2. Poroelastic Modeling and ΔCFS Calculation

To investigate the predominant triggering mechanism, we conduct poroelastic modeling that takes into account the interaction between pore pressure change (ΔP) and rock matrix deformation. We use the COMSOL Multiphysics® software (version 5.3a) to model the evolution of pore pressure and poroelastic stress surrounding the two HF horizontal wells. COMSOL Multiphysics® software employs the finite-element algorithm to simulate the fluid-solid coupling in a realistic scenario, thus we can estimate the pore pressure and poroelastic stress simultaneously. In this study, we apply the solid mechanism module and Darcy's fluid flow module to simulate the coupling process. The technical details of poroelastic modeling are given in Text S3 in Supporting Information S1.

The ΔCFS has been commonly used to study the earthquake triggering process (Deng et al., 2016; Stein, 1999). After we obtain the stress tensor and pore pressure change from the COMSOL model, then we use the following equation to calculate the ΔCFS resolved on the specific fault plane (Xu et al., 2010):

$$\begin{aligned}\Delta CFS =& \sin\lambda\left[-\frac{1}{2}\sin^2\phi(\sin(2\tilde{\delta})\sigma^{11}+\frac{1}{2}\sin(2\phi)\sin(2\tilde{\delta})\sigma^{12}+\sin\phi\cos(2\tilde{\delta})\sigma^{13}\right.\\ &\left.-\frac{1}{2}\cos^2\phi\sin(2\tilde{\delta})\sigma^{22}-\cos\phi\sin(2\tilde{\delta})\sigma^{23}+\frac{1}{2}\sin(2\tilde{\delta})\sigma^{33}\right]\\ &+\cos\lambda\left[-\frac{1}{2}\sin(2\phi)\sin\tilde{\delta}\sigma^{11}+\cos(2\phi)\sin\tilde{\delta}\sigma^{12}+\cos\phi\cos\tilde{\delta}\sigma^{13}\right.\\ &\left.+\frac{1}{2}\sin(2\phi)\sin\tilde{\delta}\sigma^{22}+\sin\phi\cos\tilde{\delta}\sigma^{23}\right]+\mu\left[\sin^2\phi\sin^2\tilde{\delta}\sigma^{11}-\sin(2\phi)\sin^2\tilde{\delta}\sigma^{12}\right.\\ &\left.-\sin\phi\sin(2\tilde{\delta})\sigma^{13}+\cos^2\phi\sin^2\tilde{\delta}\sigma^{22}+\cos\phi\sin(2\tilde{\delta})\sigma^{23}+\cos^2\phi\sigma^{33}+\Delta P\right]\end{aligned} \quad (1)$$

where $\mu = 0.6$ is the friction coefficient, ϕ, $\tilde{\delta}$, and λ are the strike, dip, and rake of the receiver fault, respectively, σ^{ij} is the stress tensor, where i, $j = 1, 2, 3$ are the 3D components in the Cartesian coordinate system and ΔP is the pore pressure change. Based on the Coulomb failure criteria, seismic slip is promoted for a positive ΔCFS, and vice versa (King et al., 1994).

3. Results

3.1. A High-Resolution 3D Pattern of IIE Migration

Based on the results of waveform analysis (Section 2.1), 20 out of 69 events are found with high CC (>0.75) and near-identical waveforms, implying that they have ruptured on similar fault structures with similar focal mechanisms. Overall, the similarity matrix of these near-identical events shows two high CC patches (Figure S3a) – one corresponds to the earlier events in the east sequence and the other to the later events in the west sequence (Figure 2). Such a two-patch pattern is consistent with the two main near-vertical fault structures (Figure 2) inferred from earthquake focal mechanisms (Schultz et al., 2017). According to the "flower structure" model, these two near-vertical faults may merge together in the basement (Wang et al., 2017). The remaining 49 poorly correlated events are generally small (overall Mw $\leq$ 1, Figure S4) and likely to have occurred on the nearby tiny fractures with possibly different orientations and/or focal mechanisms.

It is worth noting that the event magnitudes increase with focal depth for both the east and west sequences (Figure 2). Most of the relatively larger events appear to have occurred near/in the crystalline basement, possibly due to the varying degrees of fault maturity at different depths (Kozłowska et al., 2018). In comparison, there is no significant event immediately above or below the HF-targeted Duvernay shale formation (Figure 2). It appears that the aseismic region can extend up to 200 m surrounding the horizontal wells (Eyre, Eaton, Garagash, et al., 2019; Guglielmi et al., 2015).

The spatiotemporal evolution of the near-identical on-fault events (colored circles in Figure 2) clearly shows how the seismicity migrates in a 3D way: first in the east from shallow to deep, then shifting to the west, finally from deep to shallow. The seismicity migration, along with the huge fluid loss (Bao & Eaton, 2016), inherently implies the migration of the leaked fluid along pre-existing geological faults (e.g., Chen et al., 2018). Although the east sequence falls out of the target fracturing region (which is usually within a few hundred meters of the well), it is highly likely that a direct fluid connection exists between the injection well and triggered seismicity through permeable pathways. Such an inference is supported by many other cases documented in the literature (Davies et al., 2013; Galloway et al., 2018; Igonin et al., 2020; Wolhart et al., 2006) where the maximum fluid communication distance can be as far as ~1 km (Fu & Dehghanpour, 2020; Igonin et al., 2020; Wilson et al., 2018). The uppermost part of the east sequence fault seems to be aseismic, possibly due to the close proximity to the injection area (De Barros et al., 2016; Guglielmi et al., 2015) and/or high clay and organic content in the shale formation that favors stable sliding (Eyre, Eaton, Garagash, et al., 2019; Kohli & Zoback, 2013). Upon fluid injection, the fault permeability in the vicinity of the fluid channel may increase dramatically during the aseismic period (Guglielmi et al., 2015) which, in turn, facilitates rapid downward fluid pressure migration, eventually leading to seismic failures toward the basement. The fluid pressure then migrates from east to west through faults in the basement as evident from the timing and location of the induced seismicity. Finally, the fluid pressure may migrate vertically upward along the west sequence fault, as hinted by the seismicity pattern (Birdsell et al., 2015; Haagenson & Rajaram, 2020). We speculate that the Mw 3.9 mainshock near the bottom of the west sequence fault may have contributed to the

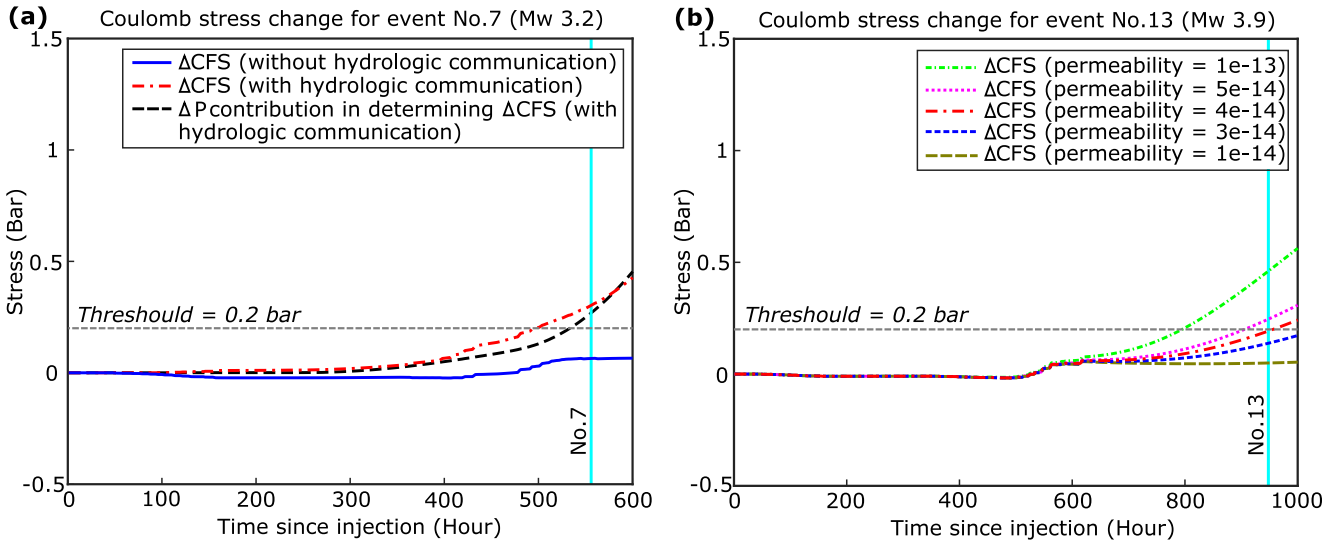

Figure 3. Poroelastic modeling results for the Mw 3.2 event (a) and Mw 3.9 event (b). Vertical cyan lines mark the origin times of the two earthquakes. Note for (b), the results of using a permeability lower than 1×10^{-14} m^2 are nearly identical to that of 1×10^{-14} m^2 and hence are not displayed for simplicity. In such low permeability cases, the ΔP contribution in determining ΔCFS for the Mw 3.9 event is negligible as the fluid pressure can not reach the west sequence fault for the observed time scale. The corresponding ΔP contributions of using different permeabilities in (b) are given in Figure S6.

upward fluid pressure migration by creating permeable and dilated pathways in the fault zone (Ruhl et al., 2016; Shelly et al., 2015). Furthermore, the lack of typical Omori-type aftershock sequence after the Mw 3.9 mainshock (Bao & Eaton, 2016) provides another piece of evidence pointing to the involvement of an external force, namely the fluid pressure from the east, in the seismogenic process on the west sequence fault (Lei et al., 2017, 2019).

In summary, in contrast to the conventional wisdom that the geomechanical effects due to fluid injection migrate outward from the injection site, our results reveal a high-resolution, complex 3D pattern of IIE migration that can go both outward and inward as controlled by local fault architecture and its hydrogeological properties. The pore pressure build-up due to rapid fluid pressure migration has caused the Mw 3.2 earthquake on the east sequence fault and the later Mw 3.9 event on the west (Figure 2). This first-outward-then-inward sequence highlights the significance of hydrologic networks in facilitating fluid pressure migration and the associated seismic failure. However, event No. 1 (Mw 1.98) appears to be an exception. It occurred very early (soon after the start of stage 17 of well 2 in P2, Figure 1b), not on the east sequence fault but the west. The hypocenter is close to event No. 11 as evident by both high CC values (Figure S3a) and precise hypocenter locations (Figure 2). Given the timing and location, event No. 1 may have been caused by poroelastic effects rather than a pore pressure perturbation. We note that the poroelastic effects may have also contributed to the occurrences of some uncorrected small events on nearby fractures or subsidiary faults during the HF stimulation (Bao & Eaton, 2016). To better characterize the poroelastic effects on the seismogenesis of IIE, we conduct quantitative geomechanical simulations with realistic injection parameters and the results are presented in the next section.

3.2. Delayed Triggering Due to Pore Pressure Build-Up

We verify the hypothesis of the pore pressure build-up being the predominant triggering mechanism through poroelastic modeling (Section 2.2). In the model, we consider two scenarios for the east sequence fault: one where the near-vertical east sequence fault intersects the inferred horizontal fluid channel, and the other where it does not (Figure 2). Our model results indicate that the ΔCFS due to poroelastic effects alone (i.e., without hydrologic communication) is only ~0.06 bar (Figure 3a). Such a small change is likely insufficient to trigger the Mw 3.2 event on the east sequence fault as it is significantly below the triggering threshold (0.2 bar) adopted by previous studies (e.g., Fischer et al., 2008; Wang et al., 2021). Instead, allowing fluid pressure migration to the seismogenic east sequence fault can explain the observations very well. Figure 3a clearly shows that the ΔP is the largest contributor to ΔCFS in elevating the local stress to a level sufficient to cause the Mw 3.2 event. The dominance of ΔP over poroelastic effects in triggering earthquakes has also been documented elsewhere (e.g., Zhai et al., 2019). We further tested a range of physically reasonable permeability values (Cappa, 2009; Farrell

et al., 2014) for the inferred near-horizontal basement fault that facilitates rapid fluid pressure migration from the east sequence fault toward the west. A minimum permeability of 4×10^{-14} m^2, about four orders higher than that of the low-permeability country rock (10^{-18} m^2, Table S1), is found to be required to cause seismic failures on the west sequence fault for the observed time scale (Figure 3b). Such a high permeability value is consistent with the laboratory results of well-developed fault damage zones ($10^{-16} - 10^{-14}$ m^2) that lead to rapid fluid flow (Evans et al., 1997). Thus, we conclude that the pore pressure build-up associated with fluid pressure migration is the key mechanism that triggered the 2015 Fox Creek earthquake sequence and that the complex 3D spatiotemporal pattern of hypocenters is dictated by the local hydrogeological setting. Although we do not have direct evidence for the existence of fluid pathways, our pore pressure triggering hypothesis appears to explain the 3D spatiotemporal distribution of the on-fault events better than previous models. Finally, we note that the poroelastic effects may play an important role in enhancing the overall seismicity rate (Zhai et al., 2019), especially for those uncorrelated small earthquakes. However, exactly how such effects evolve with time and/or space that eventually become negligible remains to be quantified. A detailed simulation with realistic physical conditions may be able to address this important question but is beyond the scope of this study.

4. Interpretation and Implications

4.1. Reactivation of Fault Segments by Fluid Injection

Previous studies have suggested that the hosting fault must be critically stressed for relatively large ($M > 2$) IIE to occur (Atkinson et al., 2020). However, our observations suggest that the east sequence fault was likely not critically stressed before stimulation. The magnitudes of the earthquakes on the east sequence fault show an overall increasing trend with time (bottom panel in Figure 1b), indicating that the fault has become more unstable. The largest event in the east sequence (event No. 7) occurred ~3 days after event No. 0. The ~3-day delay time might suggest that stage stimulation can dramatically alter the stress state from non-critical to critical over an extremely short period (on the order of days), in contrast to the tectonic loading cycle (on the order of tens/hundreds of years).

It is worth noting that, about one year later, an Mw 4.1 earthquake was induced by HF slightly to the south of the Mw 3.9 event on the west sequence fault (Figure 1a; Eyre, Eaton, Garagash, et al., 2019, Eyre, Eaton, Zecevic, et al., 2019; Wang et al., 2017). These two events share near-identical focal mechanisms (Figure 1a) and waveforms (Figure S3b), have adjacent locations (epicenters less than 1.5 km apart, and similar depths at ~4 km; Eyre, Eaton, Zecevic, et al., 2019; Schultz et al., 2017), and both occurred after the completion of HF operations with potentially significant fluid leakage (Bao & Eaton, 2016; Eyre, Eaton, Zecevic, et al., 2019). Thus, the two large events are most likely to have occurred on two adjacent segments of the same N-S striking fault. Having two nearby ruptures of limited size instead of rupturing the whole west sequence fault at once suggests that the earthquake triggering effect due to HF stimulation can be very localized. Moreover, Shen, Schmitt, and Schultz (2019) and Shen, Schmitt, and Haug (2019) establish a quantitative model for the state of stress within the crust of the Fox Creek area. Based on the Mohr-Coulomb stability criterion, their fault slip tendency analysis indicates that the west sequence fault is likely well below the critical state. They conclude that hydraulic connection between fault segments and HF probably exists and is responsible for the pore pressure increase required to trigger local earthquakes on pre-existing faults. These results are consistent with our inference that the current geomechanical state of the west sequence fault may not be able to facilitate a long rupture. Other factors, such as the heterogeneities in fault properties and/or deviatoric stress conditions (Gischig, 2015), could also affect the final size of a seismic event but will require further investigation to confirm.

Considering the facts that (a) most injection operations are not seismogenic (Atkinson et al., 2016; Rubinstein & Mahani, 2015; Schultz et al., 2017, 2020; Weingarten et al., 2015), (b) events triggered by poroelastic effects are usually of small magnitudes (Deng et al., 2016; Kozłowska et al., 2018; Yu et al., 2019), (c) the elevation of pore pressure is widely considered to be the primary cause of HF-related IIE with $M \geq 4$ (Lei et al., 2019; Peña Castro et al., 2020; Schultz & Wang, 2020; Wang et al., 2020, 2021), and (d) many $M \geq 4$ IIE exhibit significant time delay relative to the start of the corresponding HF stimulation (Lei et al., 2017; Peña Castro et al., 2020; Schultz et al., 2017, 2020; Schultz & Wang, 2020; Wang et al., 2020), we speculate that the number of critically stressed, large intraplate faults is likely to be very limited, and that reactivation of such faults requires sufficient pore-pressure accumulation. However, we acknowledge the limitation of our case study. Whether our speculation can be generalized to other IIE cases remains to be tested.

4.2. Delayed Triggering of Relatively Large IIE

Taking advantage of the high-resolution distribution of hypocenters and complete HF stimulation database, our study reveals that a complex 3D source migration process with the delay of relatively large earthquakes is controlled by the local hydrogeological setting. Numerical modeling demonstrates that poroelastic effects alone (i.e., without direct hydrological connection) are insufficient to activate the east sequence fault. Instead, the delayed occurrence of two relatively large events (i.e., Mw 3.2 and Mw 3.9) on the time scale of days to weeks can be well-explained by the pore-pressure build-up along the complex local fault system involving an initially outward path at the shallow depth and a later inward one at a greater depth. Although the actual fluid channel and fault architecture could be even more complicated than what we have assumed (Figure 2), our model succeeds in explaining the IIE migration process to the first order.

Therefore, the complexity of the hydrologic network determines whether and how fast the fluid can reach the fault; and the current stress state of the hosting fault determines how long it takes for pore-pressure build-up to facilitate seismic failure. This might explain why no relatively large (i.e., $M \geq 4$) IIE thus far occur at the onset of HF stimulation. Instead, they tend to occur near the end of, or even after the stage stimulation with a wide range of time delays (e.g., Lei et al., 2017; Peña Castro et al., 2020; Schultz et al., 2020, 2017; Schultz & Wang, 2020; Wang et al., 2017).

4.3. Seismogenic Versus Aseismogenic Injection Operations

Direct fluid communication should be geologically rare (Galloway et al., 2018). Whether earthquakes can be triggered by an injection operation depends on: (a) the probability of connecting the injection to a pre-existing seismogenic fault, and (b) whether the amount of injected fluid is sufficient to bring the fault to a critical state. Even if direct fluid communication exists, the largest magnitude of triggered events will depend on both the dimension of the pre-existing fault and the cumulative volume of injected fluid (Schultz et al., 2018). Meeting all these conditions may be statistically demanding, and thus can explain why the majority of seismogenic wells do not produce large felt IIE. This essentially agrees with the Gutenberg-Richter law that smaller earthquakes occur much more frequently than larger ones.

5. Discussion and Conclusions

Waveform similarity has been a powerful seismological tool recently to study earthquake source characteristics (Schultz et al., 2014, 2020). While there are increasing evidence that waveform CC alone cannot reliably distinguish repeating earthquakes from neighboring events (e.g., Ellsworth & Bulut, 2018; Gao et al., 2021), nearly identical waveforms are useful in identifying nearby earthquakes with similar focal mechanisms. In fact, using single-station CC values to identify earthquakes with similar origins has been a common practice in previous studies, especially for areas with limited station availability (e.g., Buurman et al., 2013; Cauchie et al., 2020; Gao & Kao, 2020; Hayward & Bostock, 2017; L. Li et al., 2011; A. Li & Richards, 2003; Schaff & Richards, 2004; Schultz et al., 2015, 2017, 2014; Yamada et al., 2016). We have tried different CC threshold values in our hierarchical clustering analysis, and the results are all similar. Although our cross-correlation and clustering analyses are based on single-station data, the overall match of the similarity matrix of the near-identical events (Figure S3a) and their hypocenter locations (Figure 2) demonstrates the effectiveness of our approach.

We take a more conservative approach in the investigation of the predominant triggering mechanism of IIE by assuming a triggering threshold of $\Delta CFS = 0.2$ bar (e.g., Fischer et al., 2008; Wang et al., 2021). Some studies have considered a lower value of 0.1 bar to define the triggering threshold (e.g., King et al., 1994; Stein, 1999). Regardless of which triggering threshold (0.1 or 0.2 bar) is used, the ΔCFS due to poroelastic effects alone is much smaller (0.06 bar, Figure 3a) and hence is insufficient to trigger the Mw 3.2 event on the east sequence fault. We conclude that the poroelastic effects are at most a contributor to triggering the 2015 Fox Creek earthquake sequence, whereas rapid pore-pressure build-up through permeable pathways may play a more important role.

As fluid migration is dictated by the pressure gradient (i.e., from high-to low-pressure regimes), the increasing hydrostatic pressure with depth (Figure S5) would imply that fluid movement is easier to go upward than downward. In the context of anthropogenic activities (including both HF and WD), however, earthquakes that occur

both above and below injection depths, presumably associated with upward or downward pressure migration, respectively, have been documented in the literature (e.g., Eyre, Eaton, Garagash, et al., 2019; Haffener et al., 2018; Keranen et al., 2013; Peña Castro et al., 2020; Schoenball & Ellsworth, 2017). In our case, the spatiotemporal evolution of observed IIE suggests that the pressure migration can go both downward (the east sequence) and upward (the west sequence, Figure 2) in a 3D loop depending on the local hydrogeological setting and fault distribution. Although the pore pressure in the Duvernay may be slightly lower than that in the basement (presumably by a few MPa) before injection, the very high injection pressure of HF stimulations (on the order of several tens of MPa, Bao & Eaton, 2016) should be more than sufficient to facilitate downward pressure migration if hydraulic connections to the basement exist. Thus, the hypothesized 3D pressure migration path in our model is not only consistent with detailed seismic observations (Section 3.1) but also validated by time-dependent poroelastic modeling of various hydrological scenarios (Section 3.2).

Although much of our analysis focuses on the 2015 Mw 3.9 Fox Creek earthquake sequence, the findings can give insights into the detailed pore-pressure triggering process of relatively large IIE elsewhere. To summarize, our study reveals that (a) poroelastic effects of HF stimulation might contribute to the occurrence of IIE, but are probably insufficient to activate a large fault segment not critically stressed, (b) the effect of HF can be very localized due to its relatively small volume, but a rapid pore-pressure build-up can load fault segments to produce large felt IIE if adequate hydrological paths exist, and (c) the spatiotemporal distribution of IIE can exhibit a very complicated 3D pattern depending on the specific local hydrogeological setting. Therefore, mapping pre-existing geological faults and avoiding direct hydrologic connection to them may be of paramount importance in mitigating short-term seismic hazards from IIE. Precise and accurate assessment of the state of stress of local fault systems is probably the key step in the strategy of maximizing the economic benefit of HF operations and minimizing the potential impact on the safety of local communities and infrastructure.

Data Availability Statement

Waveform data used in this study were downloaded from the Incorporated Research Institutions for Seismology (http://ds.iris.edu/ds/nodes/dmc/forms/breqfast-request/, last accessed July 2020) with the network code RV and station name BRLDA (Schultz & Stern, 2015). Seismic data are processed with Obspy (Beyreuther et al., 2010). Injection data (Table S2) utilized for the poroelastic modeling were supplied by the Alberta Energy Regulator and can be ordered at http://www1.aer.ca/ProductCatalogue/197.html by specifying the Unique Well Identifiers (UWI). Figures are made with Matplotlib (Hunter, 2007) and Inkscape (https://inkscape.org).

Acknowledgments
We thank Editor-in-Chief Harihar Rajaram, Mirko van der Baan, and two anonymous reviewers for their constructive comments. Insightful discussions with Fengzhou Tan, Ramin Mohammad Hosseini Dokht, Yajing Liu, and Stan Dosso are much appreciated. This study is partially supported by a University of Victoria Fellowship (DG), the Induced Seismicity Research Project of NRCan (HK), Geoscience BC (HK, BW), and a NSERC Discovery Grant (HK). This paper is NRCan contribution 20210217.

References

Atkinson, G. M., Eaton, D. W., Ghofrani, H., Walker, D., Cheadle, B., Schultz, R., et al. (2016). Hydraulic fracturing and seismicity in the western Canada sedimentary basin. *Seismological Research Letters*, *87*(3), 631–647. https://doi.org/10.1785/0220150263

Atkinson, G. M., Eaton, D. W., & Igonin, N. (2020). Developments in understanding seismicity triggered by hydraulic fracturing. *Nature Reviews Earth & Environment*, 1–14. https://doi.org/10.1038/s43017-020-0049-7

Bao, X., & Eaton, D. W. (2016). Fault activation by hydraulic fracturing in western Canada. *Science*, *354*(6318), 1406–1409. https://doi.org/10.1126/science.aag2583

Beyreuther, M., Barsch, R., Krischer, L., Megies, T., Behr, Y., & Wassermann, J. (2010). ObsPy: A Python toolbox for seismology. *Seismological Research Letters*, *81*(3), 530–533. https://doi.org/10.1785/gssrl.81.3.530

Birdsell, D. T., Rajaram, H., Dempsey, D., & Viswanathan, H. S. (2015). Hydraulic fracturing fluid migration in the subsurface: A review and expanded modeling results. *Water Resources Research*, *51*(9), 7159–7188. https://doi.org/10.1002/2015wr017810

Buurman, H., West, M. E., & Thompson, G. (2013). The seismicity of the 2009 Redoubt eruption. *Journal of Volcanology and Geothermal Research*, *259*, 16–30. https://doi.org/10.1016/j.jvolgeores.2012.04.024

Cappa, F. (2009). Modelling fluid transfer and slip in a fault zone when integrating heterogeneous hydromechanical characteristics in its internal structure. *Geophysical Journal International*, *178*(3), 1357–1362. https://doi.org/10.1111/j.1365-246x.2009.04291.x

Cauchie, L., Lengliné, O., & Schmittbuhl, J. (2020). Seismic asperity size evolution during fluid injection: Case study of the 1993 Soultz-sous-Forêts injection. *Geophysical Journal International*, *221*(2), 968–980. https://doi.org/10.1093/gji/ggaa051

Chen, X., Haffener, J., Goebel, T. H., Meng, X., Peng, Z., & Chang, J. C. (2018). Temporal correlation between seismic moment and injection volume for an induced earthquake sequence in central Oklahoma. *Journal of Geophysical Research: Solid Earth*, *123*(4), 3047–3064. https://doi.org/10.1002/2017jb014694

Davies, R., Foulger, G., Bindley, A., & Styles, P. (2013). Induced seismicity and hydraulic fracturing for the recovery of hydrocarbons. *Marine and Petroleum Geology*, *45*, 171–185. https://doi.org/10.1016/j.marpetgeo.2013.03.016

De Barros, L., Daniel, G., Guglielmi, Y., Rivet, D., Caron, H., Payre, X., et al. (2016). Fault structure, stress, or pressure control of the seismicity in shale? Insights from a controlled experiment of fluid-induced fault reactivation. *Journal of Geophysical Research: Solid Earth*, *121*(6), 4506–4522. https://doi.org/10.1002/2015jb012633

Deng, K., Liu, Y., & Harrington, R. M. (2016). Poroelastic stress triggering of the December 2013 Crooked Lake, Alberta, induced seismicity sequence. *Geophysical Research Letters*, *43*(16), 8482–8491. https://doi.org/10.1002/2016gl070421

Ellsworth, W. L., & Bulut, F. (2018). Nucleation of the 1999 Izmit earthquake by a triggered cascade of foreshocks. *Nature Geoscience*, *11*(7), 531–535. https://doi.org/10.1038/s41561-018-0145-1

Evans, J. P., Forster, C. B., & Goddard, J. V. (1997). Permeability of fault-related rocks, and implications for hydraulic structure of fault zones. *Journal of Structural Geology*, *19*(11), 1393–1404. https://doi.org/10.1016/s0191-8141(97)00057-6

Eyre, T. S., Eaton, D. W., Garagash, D. I., Zecevic, M., Venieri, M., Weir, R., & Lawton, D. C. (2019). The role of aseismic slip in hydraulic fracturing–induced seismicity. *Science Advances*, *5*(8), eaav7172. https://doi.org/10.1126/sciadv.aav7172

Eyre, T. S., Eaton, D. W., Zecevic, M., D'Amico, D., & Kolos, D. (2019). Microseismicity reveals fault activation before M w 4.1 hydraulic-fracturing induced earthquake. *Geophysical Journal International*, *218*(1), 534–546. https://doi.org/10.1093/gji/ggz168

Farrell, N. J. C., Healy, D., & Taylor, C. W. (2014). Anisotropy of permeability in faulted porous sandstones. *Journal of Structural Geology*, *63*, 50–67. https://doi.org/10.1016/j.jsg.2014.02.008

Fasola, S. L., Brudzinski, M. R., Skoumal, R. J., Langenkamp, T., Currie, B. S., & Smart, K. J. (2019). Hydraulic fracture injection strategy influences the probability of earthquakes in the Eagle Ford shale play of South Texas. *Geophysical Research Letters*, *46*(22), 12958–12967. https://doi.org/10.1029/2019gl085167

Fischer, A. D., Peng, Z., & Sammis, C. G. (2008). Dynamic triggering of high-frequency bursts by strong motions during the 2004 Parkfield earthquake sequence. *Geophysical Research Letters*, *35*(12). https://doi.org/10.1029/2008gl033905

Fu, Y., & Dehghanpour, H. (2020). How far can hydraulic fractures go? A comparative analysis of water flowback, tracer, and microseismic data from the Horn river basin. *Marine and Petroleum Geology*, *115*, 104259. https://doi.org/10.1016/j.marpetgeo.2020.104259

Galloway, E., Hauck, T., Corlett, H., Pană, D., & Schultz, R. (2018). Faults and associated karst collapse suggest conduits for fluid flow that influence hydraulic fracturing-induced seismicity. *Proceedings of the National Academy of Sciences*, *115*(43), E10003–E10012. https://doi.org/10.1073/pnas.1807549115

Gao, D., & Kao, H. (2020). Optimization of the match-filtering method for robust repeating earthquake detection: The multisegment cross-correlation approach. *Journal of Geophysical Research: Solid Earth*, *125*(7), e2020JB019714. https://doi.org/10.1029/2020jb019714

Gao, D., Kao, H., & Wang, B. (2021). Misconception of waveform similarity in the identification of repeating earthquakes. *Geophysical Research Letters*, *48*(13), e2021GL092815.

Gischig, V. S. (2015). Rupture propagation behavior and the largest possible earthquake induced by fluid injection into deep reservoirs. *Geophysical Research Letters*, *42*(18), 7420–7428. https://doi.org/10.1002/2015gl065072

Guglielmi, Y., Cappa, F., Avouac, J. P., Henry, P., & Elsworth, D. (2015). Seismicity triggered by fluid injection–induced aseismic slip. *Science*, *348*(6240), 1224–1226. https://doi.org/10.1126/science.aab0476

Haagenson, R., & Rajaram, H. (2020). Seismic diffusivity: The influence of fracture networks on the patterns of induced seismicity. In *EGU General Assembly Conference Abstracts*.

Haffener, J., Chen, X., & Murray, K. (2018). Multiscale analysis of spatiotemporal relationship between injection and seismicity in Oklahoma. *Journal of Geophysical Research: Solid Earth*, *123*(10), 8711–8731. https://doi.org/10.1029/2018jb015512

Hayward, T. W., & Bostock, M. G. (2017). Slip behavior of the queen Charlotte plate boundary before and after the 2012, MW 7.8 Haida Gwaii earthquake: Evidence from repeating earthquakes. *Journal of Geophysical Research: Solid Earth*, *122*(11), 8990–9011. https://doi.org/10.1002/2017jb014248

Hunter, J. D. (2007). Matplotlib: A 2D graphics environment. *Computing in Science & Engineering*, *9*(3), 90–95. https://doi.org/10.1109/mcse.2007.55

Igarashi, T., Matsuzawa, T., & Hasegawa, A. (2003). Repeating earthquakes and interplate aseismic slip in the northeastern Japan subduction zone. *Journal of Geophysical Research*, *108*(B5). https://doi.org/10.1029/2002jb001920

Igonin, N., Verdon, J. P., Kendall, J. M., & Eaton, D. W. (2020). Large-scale fracture systems are permeable pathways for fault activation during hydraulic fracturing. *Journal of Geophysical Research: Solid Earth*. *126*(3), e2020JB020311.

Jones, E., Oliphant, T., & Peterson, P. (2001). *SciPy: Open source scientific tools for Python*.

Keranen, K. M., Savage, H. M., Abers, G. A., & Cochran, E. S. (2013). Potentially induced earthquakes in Oklahoma, USA: Links between wastewater injection and the 2011 Mw 5.7 earthquake sequence. *Geology*, *41*(6), 699–702. https://doi.org/10.1130/g34045.1

King, G. C., Stein, R. S., & Lin, J. (1994). Static stress changes and the triggering of earthquakes. *Bulletin of the Seismological Society of America*, *84*(3), 935–953.

Kohli, A. H., & Zoback, M. D. (2013). Frictional properties of shale reservoir rocks. *Journal of Geophysical Research: Solid Earth*, *118*(9), 5109–5125. https://doi.org/10.1002/jgrb.50346

Kozłowska, M., Brudzinski, M. R., Friberg, P., Skoumal, R. J., Baxter, N. D., & Currie, B. S. (2018). Maturity of nearby faults influences seismic hazard from hydraulic fracturing. *Proceedings of the National Academy of Sciences*, *115*(8), E1720–E1729.

Lei, X., Huang, D., Su, J., Jiang, G., Wang, X., Wang, H., et al. (2017). Fault reactivation and earthquakes with magnitudes of up to Mw4. 7 induced by shale-gas hydraulic fracturing in Sichuan Basin, China. *Scientific Reports*, *7*(1), 1–12. https://doi.org/10.1038/s41598-017-08557-y

Lei, X., Wang, Z., & Su, J. (2019). The December 2018 ML 5.7 and January 2019 ML 5.3 earthquakes in South Sichuan basin induced by shale gas hydraulic fracturing. *Seismological Research Letters*, *90*(3), 1099–1110. https://doi.org/10.1785/0220190029

Li, A., & Richards, P. G. (2003). Using earthquake doublets to study inner core rotation and seismicity catalog precision. *Geochemistry, Geophysics, Geosystems*, *4*(9). https://doi.org/10.1029/2002gc000379

Li, L., Chen, Q. F., Niu, F., & Su, J. (2011). Deep slip rates along the Longmen Shan fault zone estimated from repeating microearthquakes. *Journal of Geophysical Research*, *116*(B9). https://doi.org/10.1029/2011jb008406

Peña Castro, A. F., Roth, M. P., Verdecchia, A., Onwuemeka, J., Liu, Y., Harrington, R. M., & Kao, H. (2020). Stress chatter via fluid flow and fault slip in a hydraulic fracturing-induced earthquake sequence in the Montney formation, British Columbia. *Geophysical Research Letters*, *47*(14), e2020GL087254.

Rubinstein, J. L., & Mahani, A. B. (2015). Myths and facts on wastewater injection, hydraulic fracturing, enhanced oil recovery, and induced seismicity. *Seismological Research Letters*, *86*(4), 1060–1067. https://doi.org/10.1785/0220150067

Ruhl, C. J., Abercrombie, R. E., Smith, K. D., & Zaliapin, I. (2016). Complex spatiotemporal evolution of the 2008 Mw 4.9 Mogul earthquake swarm (Reno, Nevada): Interplay of fluid and faulting. *Journal of Geophysical Research: Solid Earth*, *121*(11), 8196–8216. https://doi.org/10.1002/2016jb013399

Schaff, D. P., & Richards, P. G. (2004). Repeating seismic events in China. *Science*, *303*(5661), 1176–1178. https://doi.org/10.1126/science.1093422

Schoenball, M., & Ellsworth, W. L. (2017). A systematic assessment of the spatiotemporal evolution of fault activation through induced seismicity in Oklahoma and southern Kansas. *Journal of Geophysical Research: Solid Earth*, *122*(12), 10–189. https://doi.org/10.1002/2017jb014850

Schultz, R., Atkinson, G., Eaton, D. W., Gu, Y. J., & Kao, H. (2018). Hydraulic fracturing volume is associated with induced earthquake productivity in the Duvernay play. *Science*, *359*(6373), 304–308. https://doi.org/10.1126/science.aao0159

Schultz, R., Skoumal, R. J., Brudzinski, M. R., Eaton, D., Baptie, B., & Ellsworth, W. (2020). Hydraulic fracturing-induced seismicity. *Reviews of Geophysics*, *58*(3). e2019RG000695. https://doi.org/10.1029/2019rg000695

Schultz, R., & Stern, V. (2015). The regional Alberta observatory for earthquake studies network (RAVEN). *CSEG Recorder*, *40*(8), 34–37.

Schultz, R., Stern, V., & Gu, Y. J. (2014). An investigation of seismicity clustered near the Cordel Field, west central Alberta, and its relation to a nearby disposal well. *Journal of Geophysical Research: Solid Earth*, *119*(4), 3410–3423. https://doi.org/10.1002/2013jb010836

Schultz, R., Stern, V., Novakovic, M., Atkinson, G., & Gu, Y. J. (2015). Hydraulic fracturing and the Crooked Lake sequences: Insights gleaned from regional seismic networks. *Geophysical Research Letters*, *42*(8), 2750–2758. https://doi.org/10.1002/2015gl063455

Schultz, R., & Wang, R. (2020). Newly emerging cases of hydraulic fracturing induced seismicity in the Duvernay East Shale Basin. *Tectonophysics*, 228393. https://doi.org/10.1016/j.tecto.2020.228393

Schultz, R., Wang, R., Gu, Y. J., Haug, K., & Atkinson, G. (2017). A seismological overview of the induced earthquakes in the Duvernay play near Fox Creek, Alberta. *Journal of Geophysical Research: Solid Earth*, *122*(1), 492–505. https://doi.org/10.1002/2016jb013570

Shelly, D. R., Taira, T. A., Prejean, S. G., Hill, D. P., & Dreger, D. S. (2015). Fluid-faulting interactions: Fracture-mesh and fault-valve behavior in the February 2014 Mammoth Mountain, California, earthquake swarm. *Geophysical Research Letters*, *42*(14), 5803–5812. https://doi.org/10.1002/2015gl064325

Shen, L. W., Schmitt, D. R., & Haug, K. (2019). Quantitative constraints to the complete state of stress from the combined borehole and focal mechanism inversions: Fox Creek, Alberta. *Tectonophysics*, *764*, 110–123. https://doi.org/10.1016/j.tecto.2019.04.023

Shen, L. W., Schmitt, D. R., & Schultz, R. (2019). Frictional stabilities on induced earthquake fault planes at Fox Creek, Alberta: A pore fluid pressure dilemma. *Geophysical Research Letters*, *46*(15), 8753–8762. https://doi.org/10.1029/2019gl083566

Stein, R. S. (1999). The role of stress transfer in earthquake occurrence. *Nature*, *402*(6762), 605–609. https://doi.org/10.1038/45144

Wang, B., Harrington, R. M., Liu, Y., Kao, H., & Yu, H. (2020). A study on the largest hydraulic-fracturing-induced earthquake in Canada: Observations and static stress-drop estimation. *Bulletin of the Seismological Society of America*, *110*(5), 2283–2294. https://doi.org/10.1785/0120190261

Wang, B., Verdecchia, A., Kao, H., Harrington, R. M., Liu, Y., & Yu, H. (2021). *A study on the largest hydraulic fracturing induced earthquake in Canada: Numerical modeling and triggering mechanism*. Bulletin of the Seismological Society of America.

Wang, R., Gu, Y. J., Schultz, R., Zhang, M., & Kim, A. (2017). Source characteristics and geological implications of the January 2016 induced earthquake swarm near Crooked Lake, Alberta. *Geophysical Journal International*, *210*(2), 979–988. https://doi.org/10.1093/gji/ggx204

Weingarten, M., Ge, S., Godt, J. W., Bekins, B. A., & Rubinstein, J. L. (2015). High-rate injection is associated with the increase in US mid-continent seismicity. *Science*, *348*(6241), 1336–1340. https://doi.org/10.1126/science.aab1345

Wilson, M. P., Worrall, F., Davies, R. J., & Almond, S. (2018). Fracking: How far from faults? *Geomechanics and Geophysics for Geo-Energy and Geo-Resources*, *4*(2), 193–199. https://doi.org/10.1007/s40948-018-0081-y

Wolhart, S. L., Harting, T. A., Dahlem, J. E., Young, T., Mayerhofer, M. J., & Lolon, E. P. (2006). Hydraulic fracture diagnostics used to optimize development in the Jonah field. In *SPE Annual Technical Conference and exhibition*. Society of Petroleum Engineers.

Xu, C., Wang, J., Li, Z., & Drummond, J. (2010). Applying the Coulomb failure function with an optimally oriented plane to the 2008 Mw 7.9 Wenchuan earthquake triggering. *Tectonophysics*, *491*(1–4), 119–126. https://doi.org/10.1016/j.tecto.2009.09.019

Yamada, M., Mori, J., & Matsushi, Y. (2016). Possible stick-slip behavior before the Rausu landslide inferred from repeating seismic events. *Geophysical Research Letters*, *43*(17), 9038–9044. https://doi.org/10.1002/2016gl069288

Yu, H., Harrington, R. M., Liu, Y., & Wang, B. (2019). Induced seismicity driven by fluid diffusion revealed by a near-field hydraulic stimulation monitoring array in the Montney Basin, British Columbia. *Journal of Geophysical Research: Solid Earth*, *124*(5), 4694–4709. https://doi.org/10.1029/2018jb017039

Zhai, G., Shirzaei, M., Manga, M., & Chen, X. (2019). Pore-pressure diffusion, enhanced by poroelastic stresses, controls induced seismicity in Oklahoma. *Proceedings of the National Academy of Sciences*, *116*(33), 16228–16233. https://doi.org/10.1073/pnas.1819225116

References From the Supporting Information

Frohlich, C., Ellsworth, W., Brown, W. A., Brunt, M., Luetgert, J., MacDonald, T., & Walter, S. (2014). The 17 May 2012 M4. 8 earthquake near Timpson, East Texas: An event possibly triggered by fluid injection. *Journal of Geophysical Research: Solid Earth*, *119*(1), 581–593. https://doi.org/10.1002/2013jb010755

Harris, C. R., Millman, K. J., van der Walt, S. J., Gommers, R., Virtanen, P., Cournapeau, D., et al. (2020). Array programming with NumPy. *Nature*, *585*(7825), 357–362. https://doi.org/10.1038/s41586-020-2649-2

Kennett, B. L., Engdahl, E. R., & Buland, R. (1995). Constraints on seismic velocities in the Earth from traveltimes. *Geophysical Journal International*, *122*(1), 108–124. https://doi.org/10.1111/j.1365-246x.1995.tb03540.x

Laske, G., Masters, G., Ma, Z., & Pasyanos, M. (2013). Update on CRUST1. 0—A 1-degree global model of Earth's crust. *Geophysical Research Abstract*, *15*, 2658.

Machel, H. G., Buschkuehle, B. E., Michael, K., & Cidu, R. (2001). Squeegee flow in Devonian carbonate aquifers in Alberta, Canada. *Water-Rock Interaction*, *1*, 631–634.

Machel, H. G., & Cavell, P. A. (1999). Low-flux, tectonically-induced squeegee fluid flow ("hot flash") into the Rocky Mountain Foreland Basin. *Bulletin of Canadian Petroleum Geology*, *47*(4), 510–533.

Potma, K., Weissenberger, J. A., Wong, P. K., & Gilhooly, M. G. (2001). Toward a sequence stratigraphic framework for the Frasnian of the Western Canada Basin. *Bulletin of Canadian Petroleum Geology*, *49*(1), 37–85. https://doi.org/10.2113/49.1.37

Schmittbuhl, J., Karabulut, H., Lengliné, O., & Bouchon, M. (2016). Long-lasting seismic repeaters in the Central basin of the Main Marmara fault. *Geophysical Research Letters*, *43*(18), 9527–9534. https://doi.org/10.1002/2016gl070505

Schweitzer, J. (2001). HYPOSAT–An enhanced routine to locate seismic events. *Pure and Applied Geophysics*, *158*(1), 277–289. https://doi.org/10.1007/pl00001160

Waldhauser, F., & Ellsworth, W. L. (2000). A double-difference earthquake location algorithm: Method and application to the northern Hayward fault, California. *Bulletin of the Seismological Society of America*, *90*(6), 1353–1368. https://doi.org/10.1785/0120000006

Wang, R., & Kümpel, H. J. (2003). Poroelasticity: Efficient modeling of strongly coupled, slow deformation processes in multilayered half-space. *Geophysics*, *68*(2), 705–717. https://doi.org/10.1190/1.1567241

Warren-Smith, E., Chamberlain, C. J., Lamb, S., & Townend, J. (2017). High-precision analysis of an aftershock sequence using matched-filter detection: The 4 May 2015 ML 6 Wanaka earthquake, Southern Alps, New Zealand. *Seismological Research Letters*, *88*(4), 1065–1077.

Warren-Smith, E., Fry, B., Kaneko, Y., & Chamberlain, C. J. (2018). Foreshocks and delayed triggering of the 2016 MW7. 1 Te Araroa earthquake and dynamic reinvigoration of its aftershock sequence by the MW7. 8 Kaikōura earthquake, New Zealand. *Earth and Planetary Science Letters*, *482*, 265–276. https://doi.org/10.1016/j.epsl.2017.11.020

Wendte, J., Qing, H., Dravis, J. J., Moore, S. L., Stasiuk, L. D., & Ward, G. (1998). High-temperature saline (thermoflux) dolomitization of Devonian Swan Hills platform and bank carbonates, Wild River area, west-central Alberta. *Bulletin of Canadian Petroleum Geology*, *46*(2), 210–265.

Yehya, A., Yang, Z., & Rice, J. R. (2018). Effect of fault architecture and permeability evolution on response to fluid injection. *Journal of Geophysical Research: Solid Earth*, *123*(11), 9982–9997. https://doi.org/10.1029/2018jb016550